Sonodynamic therapy improves anti-tumor immune effect by increasing the infiltration of CD8+ T cells and altering tumor blood vessels in murine B16F10 melanoma xenograft

YAN PENG[1*], LIMIN JIA[1*], SHAN WANG[2], WENWU CAO[3,4] and JINHUA ZHENG[1]

[1]Department of Anatomy, Basic Medical Science College, Harbin Medical University, Harbin, Heilongjiang 150081; [2]Department of Oral Pathology, Stomatological Hospital, Harbin Medical University, Harbin, Heilongjiang 150001; [3]Condensed Matter Science and Technology Institute, and Department of Physics, Harbin Institute of Technology, Harbin, Heilongjiang 150080, P.R. China; [4]Materials Research Institute, The Pennsylvania State University, University Park, State College, PA 16802, USA

Received January 30, 2018; Accepted July 19, 2018

DOI: 10.3892/or.2018.6612

Abstract. Sonodynamic therapy (SDT) uses a combination of sonosensitizers and low-intensity therapeutic ultrasound to destroy tumor cells. However, its effects on the tumor microenvironment, particularly on the immune state, remain unknown. The purpose of the present study was to examine the capacity and potency of the antitumor immunity induced by SDT. In the present study, sonosensitizer, 5-aminolevulinic acid (5-ALA), and/or ultrasound (US) were used to treat mouse B16F10 melanoma xenograft (1.0 MHz, 0.8 W/cm^2, 10% duty cycle) and human umbilical vein endothelial cells (HUVECs; 0.87 MHz, 0.6 W/cm^2, 60% duty cycle). Various immune cells, and proteins associated with the immunoregulation such as forkhead Box P3 (Foxp3), cytotoxic T-lymphocyte associated protein 4 (CTLA-4), and CD80 were detected by immunofluorescence staining and western blotting. The effect of SDT on blood vessels which were located in the central and peripheral area of tumor tissues was observed by transmission electron microscopy, immunohistochemical and immunofluorescence staining. The effect of SDT on intercellular adhesion molecule-1 (ICAM-1) expression on HUVECs was detected by western blotting and reverse transcription-semi-quantitative polymerase chain reaction. The results revealed that SDT inhibited tumor growth and improved outcomes. The mean inhibition rate of tumor volume in the US + ALA group was 43.8% and median survival was 45 days in US + ALA group vs. 27.5 days in the control group. SDT increased the number of CD45$^+$ cells, in particular CD8$^+$ and CD68$^+$ cells and upregulated the expression of CD80 in the tumor tissues. The expression levels of Foxp3 and CTLA-4 were downregulated following SDT. The endothelial cells of tumor central were damaged, but the lumen area of the tumor peripheral vessels (TPVs) and the expression of ICAM-1 on HUVECs were increased after SDT. The results indicated that SDT improved the outcomes of melanoma-loading mice, increased the infiltration of CD8$^+$ T cells and downregulates the expression of Foxp3 and CTLA-4 in mouse melanoma tissues. Furthermore, SDT increased the lumen area of TPVs in murine xenograft and the expression of ICAM-1 on HUVECs, which may be beneficial to the transendothelial migration of immune cells and the anti-tumor immune response.

Correspondence to: Professor Jinhua Zheng, Department of Anatomy, Basic Medical Science College, Harbin Medical University, 157 Baojian Road, Harbin, Heilongjiang 150081, P.R. China
E-mail: jhzheng@ems.hrbmu.edu.cn

*Contributed equally

Key words: sonodynamic therapy, melanoma xenograft, CD8$^+$ T cells, tumor blood vessels, human umbilical vein endothelial cells, intercellular adhesion molecule-1, antitumor immunity

Introduction

Sonodynamic therapy (SDT) combines ultrasound and sonosensitizers to treat malignancies. SDT is a type of anti-cancer treatment with promising potential due to its excellent ability to selectively destroy tumor cells and maximize the protection for normal tissues, which makes the SDT method unique for treating patients with tumors in anatomical positions that are difficult to access surgically (1,2).

Previous studies have suggested that SDT induces apoptosis, autophagy, and necrosis of tumor cells (3-9). Our previous studies have demonstrated that SDT inhibits neovascularization in tumor tissues (10), enhances the pro-inflammatory response and reverses the passive properties of macrophages and dendritic cells (11). However, the effects of SDT on the immune status of the tumor microenvironment are still unknown.

The occurrence of tumor-associated immune responses is dependent mainly on the infiltration of reactive leukocytes in the tumor microenvironment (12,13). The tumor microenvironment should exhibit similar immune cell surveillance to normal tissue. However, due to the long-term exposure

of tumor-induced immune cells to the tumor microenvironment, they may directly or indirectly promote malignancy. Therefore, immune cells are often ineffective in destroying tumors because of their inability to implement their cytotoxic effector functions, which is shown by the transformation of M1-M2 type tumor-associated macrophages, and the restriction of dendritic cells in the 'immature stage' (14).

Galon *et al* (15) demonstrated that the numbers of antigen-specific immune cells within the tumor microenvironment, such as $CD8^+$ T cells, are highly relevant to the clinical prognosis (15). Morphological changes in the tumor microenvironment suggest that SDT could mitigate the declining function of macrophages and dendritic cells in both nude mice and BALB/c mice with healthy immune systems (11). As SDT can positively affect the phenotype and number of macrophages and dendritic cells within the tumor microenvironment, it was hypothesized that it is highly likely for SDT to beneficially influence the numbers and phenotype of tumor-associated immune cells, which may then improve outcomes.

In the current study, the effects of SDT on the number of immune cell subtypes and outcomes in the BALB/c mice xenograft model were investigated. In addition, it should be noted that immune cell infiltration into the tumor microenvironment occurs via the vascular system. Hence, the present study also investigated the characteristics of blood vessels involved in the transport of immune cells.

Materials and methods

Chemicals and reagents. 5-Aminolevulinic acid (5-ALA) was purchased from Sigma-Aldrich (Merck KGaA, Darmstadt, Germany). Rabbit anti-intercellular adhesion molecule (ICAM)-1 (catalog no. bs-4617R), vascular cell adhesion protein (VCAM)-1 (catalog no. bs-0396R), E-selectin (catalog no. bs-1273R), CD68 (catalog no. bs-20402R), CD4 (catalog no. bs-0647R), CD8 (catalog no. bs-0647R), CTLA-4 (catalog no. bs-1179R), Foxp3 (catalog no. bs-0269R), CD80 (catalog no. bs-2211R), CD45 (catalog no. bs-0522R) antibodies were provided by BIOSS (Beijing, China). The mouse anti-CD31 antibody (catalog no. ab24590) was from Abcam (Cambridge, UK) and the rabbit anti-β-actin antibody (catalog no. A1978 MSDS) was from Sigma-Aldrich. All other chemicals and reagents were supplied by OriGene Technologies, Inc. (Beijing, China) unless otherwise indicated.

Cell culture. Murine melanoma B16F10 cells were purchased from the Chinese Academy of Sciences, Shanghai Institute Cell Resource Center, and cultured in Roswell Park Memorial Institute 1640 medium (Hyclone; GE Healthcare Life Sciences, Logan, UT, USA) supplemented with 10% heat-inactivated fetal bovine serum, 100 U/ml penicillin, and 100 g/ml streptomycin (Gibco; Thermo Fisher Scientific, Inc., Waltham, MA, USA) at 37˚C in a 5% CO_2 humidified environment. Primary human umbilical vein endothelial cells (HUVECs) and their appropriate medium were purchased from ScienCell Research Laboratories (San Diego, CA, USA). Tissue culture flasks were pre-coated with poly-L-lysine. Cells were cultured in endothelial cell growth medium supplemented with endothelial cell growth supplement, 5% fetal bovine serum, and penicillin/streptomycin solution and maintained at 37˚C in 5% CO_2 humidified environment. HUVECs from the 2nd to 5th passage were used in all experiments.

Tumor xenograft mouse model. A total of forty-eight male BALB/c mice (weight, 12-14 g; age, 4 weeks) were purchased from Vital River Laboratories (Beijing, China). All mice were bred in dedicated pathogen-free barrier facilities in a standard animal laboratory allowing free activity and were provided with standard food and water *ad libitum*. Mice were maintained at 22-24˚C in 55% humidity, on a 12-h light/12-h dark cycle. 100 μl B16F10 cell suspension ($1x10^6$ cells/ml) was injected subcutaneously into the flanks of the mice. The mice were ready for use when the tumors reached 100 mm^3 (~5 days after inoculation). All animal protocols were approved by the Animal Care and Use Committee of Harbin Medical University (Harbin, China).

Ultrasonography. The ultrasonic device was designed and manufactured by the Harbin Institute of Technology, which contained two parts: A RIGOL DG204A function arbitrary wave form generator and a North Star Model SWA200ARF power amplifier. This machine was used as previously described (7).

Treatment protocols. In the *in vivo* experiment, 48 mice were divided randomly and equally into four groups: Control, 5-ALA (250 mg/kg body weight), sonication (US), and sonication plus 5-ALA (250 mg/kg) (US + ALA). The tumors were sonicated (1.0 MHz, 0.8W/cm^2, 10% duty cycle) for 5 min in the dark in the US group and US + ALA group four hours after intraperitoneal injection of 5-ALA. This treatment was repeated twice weekly for 2 weeks (namely, four treatments in total). Half of the mice in each group were used for histology and western blotting procedures and the other half in each group were used for survival analysis.

In the *in vitro* experiment, HUVECs were divided into four groups: Control, ALA, US, and US + ALA. In the ALA and US + ALA groups, the cells were incubated with 1 mM ALA in the dark. Instead of ALA, an equivalent quantity of medium was used for the control and US groups. After 4 h incubation, the cells in the US and US + ALA groups were exposed to ultrasound (0.87 MHz, 0.6 W/cm^2, 60% duty cycle) for 60 sec in the dark.

Evaluation of antitumor effect. Mice were examined once every 2 days after the tumor volume reached 100 mm^3. The orthogonal tumor dimensions (A and B) were measured with Vernier calipers. The tumor volume was calculated as follows: Volume=$(\pi/6)$ x A x B^2. To minimize suffering, mice were sacrificed when the primary tumor reached a diameter of 1.5 cm (death due to progressive tumor) or when the mouse had lost ≥20% of its body weight and the primary tumor was less than 1.5 cm (death due to metastatic disease). Mice were considered cured when the tumor did not return 90 days after corresponding treatment or their body weight remained normal.

Histology. Formalin-fixed (10%, overnight at 4˚C), paraffin-embedded tumor tissues were sectioned (2.5 μm), placed in series on silanized glass slides, dewaxed, and rehydrated.

Antigens were retrieved following treatment in 10 mM citrate buffer (pH 6.0) for 15 min in a pressure cooker. After rinsing with phosphate-buffered saline, the sections were immersed in 3% hydrogen peroxide solution for 10 min to block endogenous peroxidases. Non-specific binding was prevented by incubation in 5% normal goat serum for 20 min in a humidified chamber.

For immunofluorescence staining, the sections were then incubated with antibodies for CD45, CD68, CD4, CD8 (1:100 dilution) overnight at 4˚C, washed, and incubated with Alexa Fluor 488-conjugated goat anti-rabbit IgG (1:800 dilution; Abcam; catalog no. ab150117) at 37˚C for 30 min. For double staining with antibodies for CD31 and ICAM-1, VCAM-1, or E-selectin (1:100 dilution), samples were incubated at 4˚C overnight with the primary antibodies (mouse anti-mouse CD31 and rabbit anti-mouse ICAM-1, VCAM-1 or E-selectin, or mouse IgG1). Samples were then washed and incubated with Alexa Fluor 488-conjugated goat anti-mouse IgG (1:800 dilution; Abcam; catalog no. ab150117) and Alexa Fluor 405-conjugated donkey anti-rabbit IgG (1:800 dilution; Abcam; catalog no. ab175651) at 37˚C for 30 min. Images were captured with a fluorescence imaging microscope (Olympus BX51; Olympus Corporation, Tokyo, Japan) equipped with Flash Point software.

For immunohistochemical staining, the sections were incubated with antibodies for CD31 (1:100) overnight at 4˚C, washed, and incubated with secondary antibodies (immediate-use goat anti-rabbit IgG horseradish-peroxidase polymers; OriGene Technologies, Inc.; catalog no. PV-6001) at 37˚C for 30 min. Diaminobenzidine was used as a chromogen. Tissue sections were counterstained with hematoxylin at room temperature for 10 sec, dehydrated and mounted. The sections were observed under a light microscope (Olympus BX51; Olympus Corporation).

Negative control immunostaining was carried out using the same procedure except that the primary antibody was replaced by nonimmunized serum.

Western blot analyses. Fresh tissue samples and cells were lysed in radioimmunoprecipitation assay lysis buffer (Beyotime Institute of Biotechnology, Haimen, China) on ice. Protein concentrations were determined using BCA protein assay kit (Beyotime Institute of Biotechnology). Equal amounts of proteins (30 μg per lane) were separated by 10% SDS-PAGE and electrophoretically transferred onto a nitrocellulose filter membrane. After blocking in Tris-buffered saline Tween-20 (TBST) containing 5% low-fat milk at room temperature for 1.5 h, the membranes were incubated overnight at 4˚C with primary antibodies against the target proteins CD68 (1:200 dilution; BIOSS; catalog no. bs-20402R), CD4 (1:300 dilution; BIOSS; catalog no. bs-0647R), CD8 (1:350 dilution; BIOSS; catalog no. bs-0647R), CTLA-4 (1:200 dilution; BIOSS; catalog no. bs-1179R), Foxp3 (1:100 dilution; BIOSS; catalog no. bs-0269R), CD80 (1:300 dilution; BIOSS; catalog no. bs-2211R), with β-actin (1:5,000 dilution; Sigma-Aldrich, Merck KGaA; catalog no. A1978 MSDS) as loading control. After washing three times with TBST, the membranes were incubated with horseradish peroxidase-conjugated secondary antibodies (1:30,000 dilution; OriGene Technologies, Inc.; catalog no. ZB-2301) for 1 h at room temperature. After washing twice with TBST which was then removed from the membrane, ECL developing reagent (Beyotime Institute of Biotechnology) was then added to the membrane. Protein levels were detected using an ECL detection system (Tanon-5200; Tanon Technology Co., Ltd., Shanghai, China) (16). The relative abundance of each band was quantified by using Quantity One software (Bio-Rad Laboratories, Inc., Hercules, CA, USA). Data were normalized to β-actin.

Transmission electron microscopy (TEM). For TEM study, xenografts were dissected and fixed with 2.5% glutaraldehyde for 2 h. Then, they were postfixed in 1% OsO_4 at 4˚C for 2 h, and were embedded with Epon812 (EM Sciences, Washington, PA, USA) for 72 h at 60˚C. Ultrathin sections were cut (70 nm) and stained with 0.5% uranium acetate at room temperature for 30 min, followed by lead citrate, and then observed under a transmission electron microscope (JEOL 200, Hitachi, Ltd., Tokyo, Japan).

Reverse transcription-semi-quantitative polymerase chain reaction (RT-sqPCR). Total-RNA from the cultured cells was isolated using TRIzol® reagent (Sigma-Aldrich; Merck KGaA) as described in a previous work (8). To quantify ICAM-1 mRNA, first strand cDNAs were synthesized using the ImProm-II™ Reverse Transcription System (Promega Corporation, Madison, WI, USA) according to the manufacturer's protocol. The RT-PCR was performed using Go Taq® Colorless Master Mix (Promega Corporation) on an Alpha Unit Block Assembly for DNA Engine System (Bio-Rad Laboratories, Inc.). All primers were obtained from GenScript (Nanjing, China). Glyceraldehyde-3-phosphate dehydrogenase (GAPDH) was used as an endogenous control. Primers used for mRNA detection were: Forward, 5'-CTCCTGTGACCA GCCCAAGT-3' and reverse, 5'-GGCAGCGTAGGGTAAGGT TC-3' for ICAM-1 and forward, 5'-AACGGATTTGGTCGT ATTGG-3' and reverse, 5'-TGGAAGATGGTGATGGGATT-3' for GADPH. Thermocycling conditions: One cycle at 94˚C for 2 min, followed by 25 cycles at 94˚C for 30 sec, 56˚C for 40 sec, and 72˚C for 30 sec. This was followed by a single cycle at 72˚C for 5 min to facilitate final extension. PCR products were run on 1% agarose gels and visualized by AlphaDigiDoc digital camera gel imaging system (ProteinSimple, San Jose, CA, USA). The densitometry was quantified by using Quantity One software (Bio-Rad Laboratories, Inc.).

Computer-aided morphological analysis. Image-Pro Plus 6.0 (Media Cybernetics Inc. Rockville, MD, USA) was used to calculate the intensity of the detected markers. Three fields (original magnification, x400) were selected randomly and the optical densities of ICAM-1, VCAM-1, E-selectin, CD68, CD4, CD8 and CD31 were calculated. Higher integral optical density values represented higher antigen expression.

Statistical analyses. Data are presented as the mean ± standard deviation. Statistical differences were evaluated by unpaired Student's t-test or one-way analysis of variance with Bonferroni post hoc test, using SPSS software, version 20 (IBM, Armonk, NY, USA). The Kaplan-Meier curves were analyzed with the log-rank test to assess the significance of differences in the

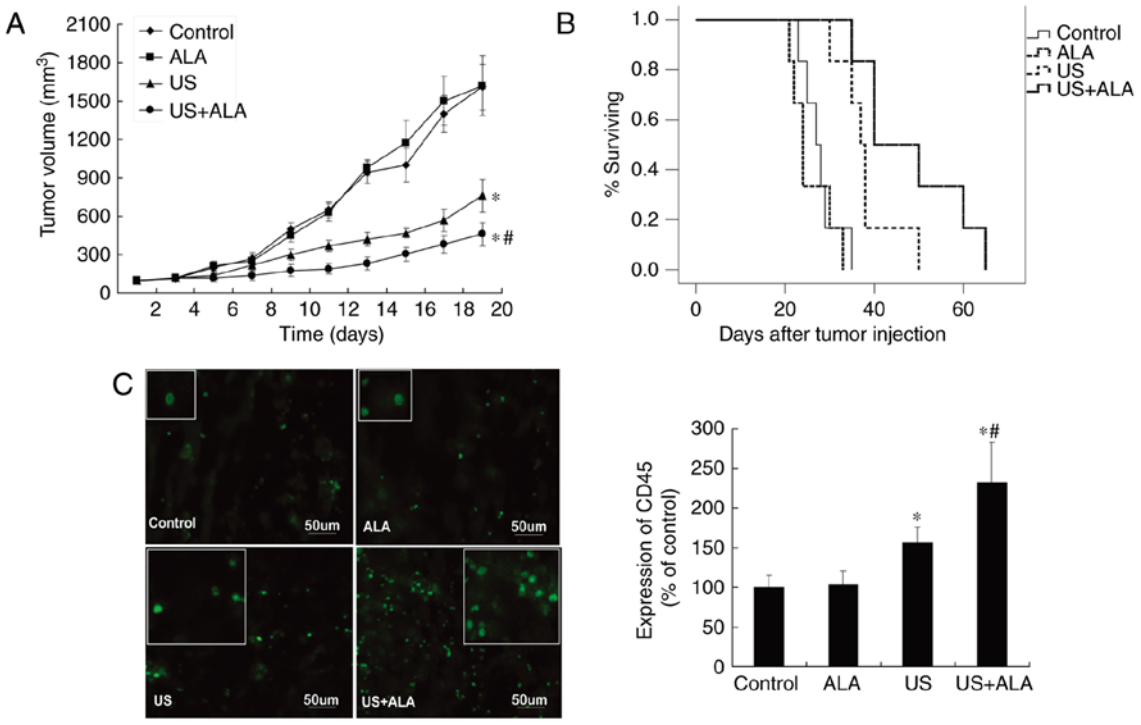

Figure 1. Effects of sonodynamic therapy on tumor growth, survival, and the number of immunocytes in tumor-bearing BALB/c mice. (A) Tumor volumes recorded during treatment. Data are presented as the mean ± standard deviation (n=6). (B) Kaplan-Meier survival (days) curves (n=6 mice per group). (C) Tumor tissues were evaluated by immunofluorescence staining with an anti-CD45 antibody. Data are presented as the mean ± standard deviation (n=6). *P<0.05 vs. control; #P<0.05 vs. US. US, sonication; ALA, 5-aminolevulinic acid.

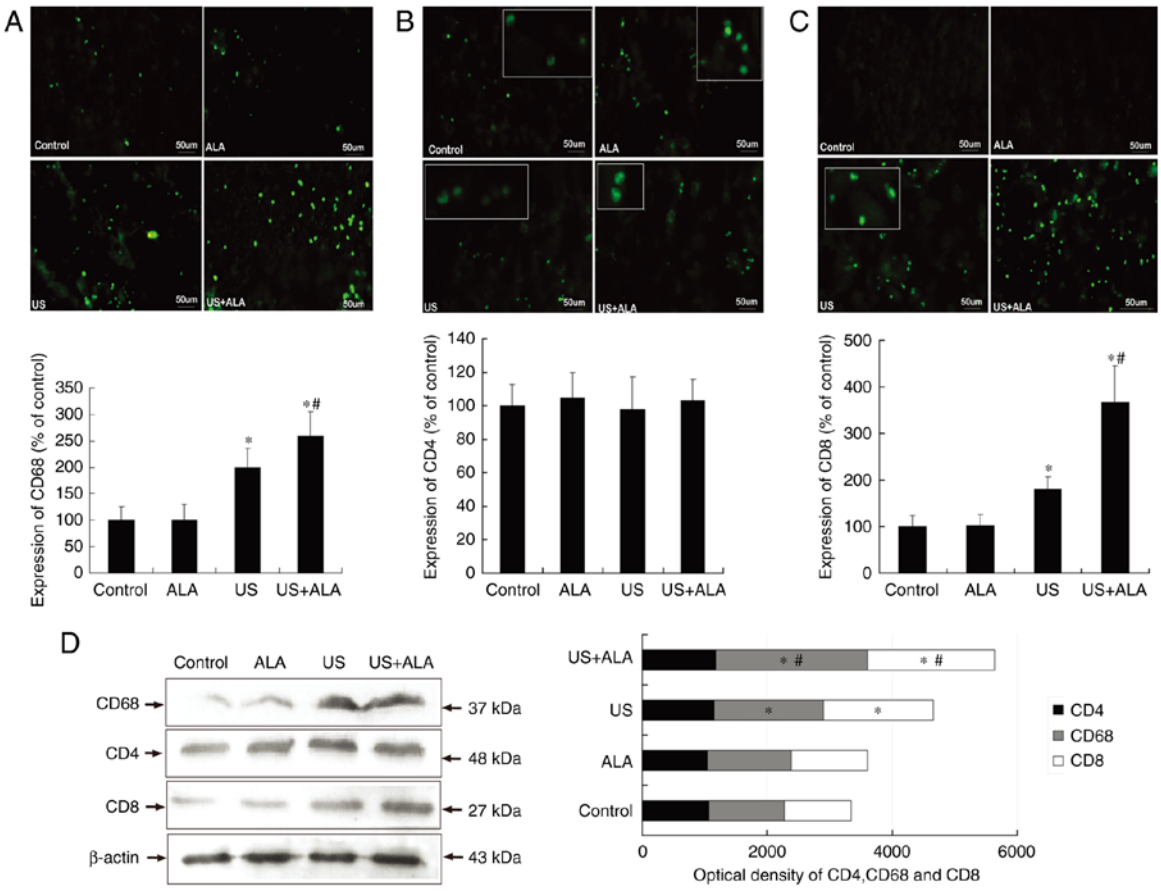

Figure 2. Effect of sonodynamic therapy on immunocytes in the tumor microenvironment. Immunofluorescence staining of tumor tissues, using rabbit (A) anti-CD68, (B) CD4 and (C) CD8. (D) Expression of CD68, CD4 and CD8 in tumor tissue samples were analyzed by western blotting. Data are presented as the mean ± standard deviation. *P<0.05 vs. control; #P<0.05 vs. US. US, sonication; ALA, 5-aminolevulinic acid.

survival rates of the mice. P<0.05 was considered to indicate a statistically significant difference.

Results

SDT inhibits growth of xenograft tumors and improves tumor-loading mice outcomes. After the four treatments, tumors were observed until the 20th day, and compared with the control group, mice treated with ALA alone exhibited no significant tumor growth suppression (ALA; P=0.617 vs. control). In contrast, the tumor growth inhibition ratios with ultrasound were 22.4% (US) and 43.8% (US + ALA), respectively (US, P=0.014; US + ALA, P<0.0001 vs. control; Fig. 1A).

Fig. 1B shows the survival curves of all four groups of mice. The median survival times for the control and ALA groups were 27.5 and 24 days (ALA; P=0.626 vs. control), respectively. The median survival times for the US and US + ALA groups were 37.5 days (US; P=0.031 vs. control) and 45 days (US + ALA; P=0.001 vs. control), respectively. Although US group achieved statistical significance, SDT still had a greater effect on the outcomes of the mice than the US treatment alone.

Effect of SDT on the number of different immune cells in the tumor microenvironment. According to Galon *et al*, a more active immune status implies a good prognosis (15). Therefore, the present study first determined the effect of SDT on changes in the total number of immune cells by using CD45 as a marker. The number of $CD45^+$ cells was not significantly different between the control and ALA groups (P=0.905). However, $CD45^+$ cell count in both the US (P=0.039) and US + ALA (P=0.009) groups were significantly increased compared with control group, however the US + ALA group demonstrated a greater increase (Fig. 1C).

In the US + ALA group, $CD68^+$ cells (ALA, P=0.973; US, P=0.013; US + ALA, P<0.001 vs. control; P=0.038 for US vs. US + ALA) and $CD8^+$ cells (ALA, P=0.957; US, P=0.037; US + ALA, P<0.0001 vs. control) (P=0.010 for US vs. US + ALA) increased significantly (Fig. 2). In addition, the extent of the increase was far greater in the US + ALA group than in the US alone group. There were no significant differences in the $CD4^+$ T cells count (Fig. 2B). In order to further confirm these findings, western blotting was performed to measure changes in the expression of CD4, CD8, and CD68 proteins. The results indicated that although the expression levels of CD8 and CD68 protein were increased in the US + ALA group, the CD4 protein level did not change after any treatment. (Fig. 2D; ALA; P=0.698, US; P=0.876, US + ALA; P=0.815 vs. control).

SDT reduces the immune tolerance of T cells. The expression levels of Foxp3 and CTLA4, which are associated with regulatory T cells and the downregulation of the immune response, were determined, although the expression level of the CD4 protein was similar in all four groups. Compared with the control group, the expression levels of Foxp3 (US; P<0.0001, US + ALA; P<0.0001 vs. control) and CTLA-4 (US; P=0.007, US + ALA; P=0.003 vs. control) proteins were reduced in the US and US + ALA groups (Fig. 3). Furthermore, the level of CD80 which is a co-stimulatory molecule related to Th1 cell activation was investigated. The results revealed

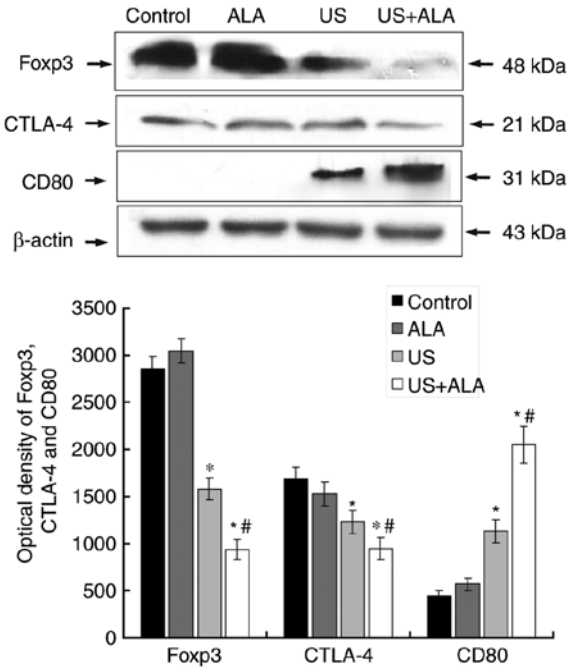

Figure 3. Expression levels of Foxp3, CTLA-4, and CD80 proteins in tumor tissue samples. Protein levels were analyzed by western blotting. Data are presented as the mean ± standard deviation. *P<0.05 vs. control; #P<0.05 vs. US. Foxp3, forkhead Box P3; CTLA-4, cytotoxic T-lymphocyte associated protein 4; US, sonication; ALA, 5-aminolevulinic acid.

that the expression of CD80 was negligible in the control and ALA groups, but increased significantly in US + ALA group (P<0.0001; Fig. 3).

Effect of SDT on blood vessels in the central and peripheral area of tumor. CD31 was used as a marker of blood vessels. Compared with the control group, the number of tumor central vessels (TCVs) was significantly reduced in US + ALA group (Fig. 4A-C). TEM revealed that the there was no damage of TCVs in control group, whereas endothelial cells of TCVs in US + ALA group were damaged with mitochondrial swelling, chromatin aggregation, and the appearance of platelets and red blood cells in proximity to the vascular endothelium (Fig. 4D and E).

Compared with the control group (1619±153.1 μm^2), the mean lumen cross-sectional area of tumor peripheral vessels (TPVs) was increased in the US + ALA group (4138 ± 379.3 μm^2; Fig. 5A and B) and this difference was statistically significant (P=0.003; Fig. 5C). TEM revealed that many lymphocytes were present in the lumen of TPVs (Fig. 5D-F). Immunofluorescence double staining results showed that ICAM-1, VCAM-1 and E-selectin, which were associated with lymphocyte adhesion, were co-expressed with vascular endothelial marker CD31 respectively in the TPVs of the US + ALA group (Fig. 5G).

Effect of SDT on ICAM-1 expression on HUVECs. To investigate whether SDT affects ICAM-1 expression on endothelial cells, the present study detected the expression level of ICAM-1 protein on HUVECs by western blotting. The results indicated that compared with the US group, the expression level of ICAM-1 protein was significantly increased in the US + ALA

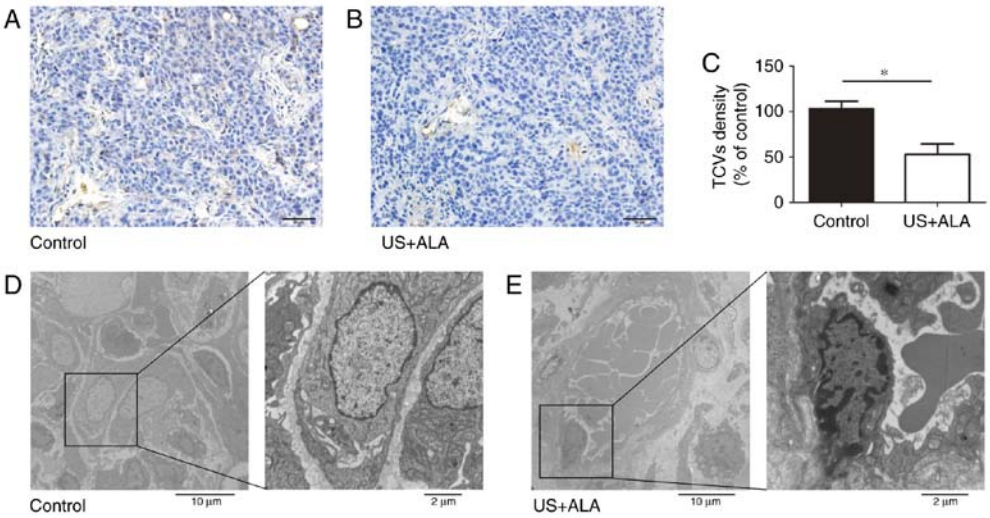

Figure 4. Effect of sonodynamic therapy on TCVs. Immunohistochemical staining of TCVs samples in (A) control and (B) US + ALA groups, using mouse anti-CD31. Scale bars, 50 μm. (C) Statistical significance was determined by an unpaired t-test. Data are presented as the mean ± standard deviation. *P<0.05 vs. control. (D and E) Transmission electron microscopy images of the TCVs in control and US + ALA groups. Black box: Vascular endothelial cells. The images on the right represent the magnified area of the box in left. TCVs, tumor center blood vessels; US, sonication; ALA, 5-aminolevulinic acid.

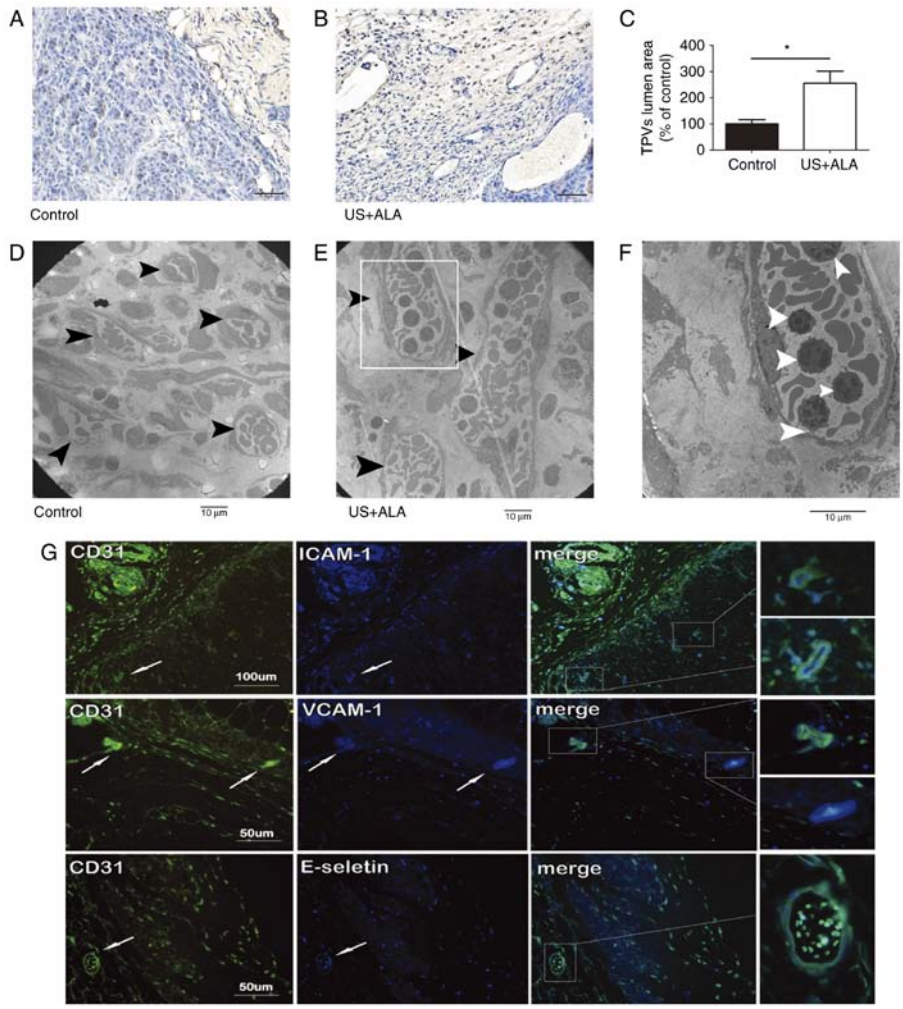

Figure 5. Effect of sonodynamic therapy on TPVs. Immunohistochemical staining of TPVs in (A) control and (B) US + ALA groups, using mouse anti-CD31. (C) Statistical significance was determined by an unpaired t-test. Data are presented as the mean ± standard deviation. *P<0.05 vs. control. (D-F) TEM images of the TPVs. Compared with the control group, the lumen diameter of TPVs (black arrowheads) in US + ALA group was increased, and many lymphocytes (white arrowheads) were shown to be present in the lumen of these vessels. (F) Magnified areas of images presented in (E). Magnification, (D and E) x2000, (F) x4000. Scale bars, 10 μm. (G) Immunofluorescence double staining of the tumor vasculatures in the US + ALA group. ICAM-1-CD31, VCAM-1-CD31, and E-selectin-CD31 were located mainly in vascular endothelial cells distributed around the tumor periphery. TPVs, tumor peripheral blood vessels; US, sonication; ALA, 5-aminolevulinic acid; ICAM-1, intercellular adhesion molecule-1; VCAM-1; vascular cell adhesion protein-1.

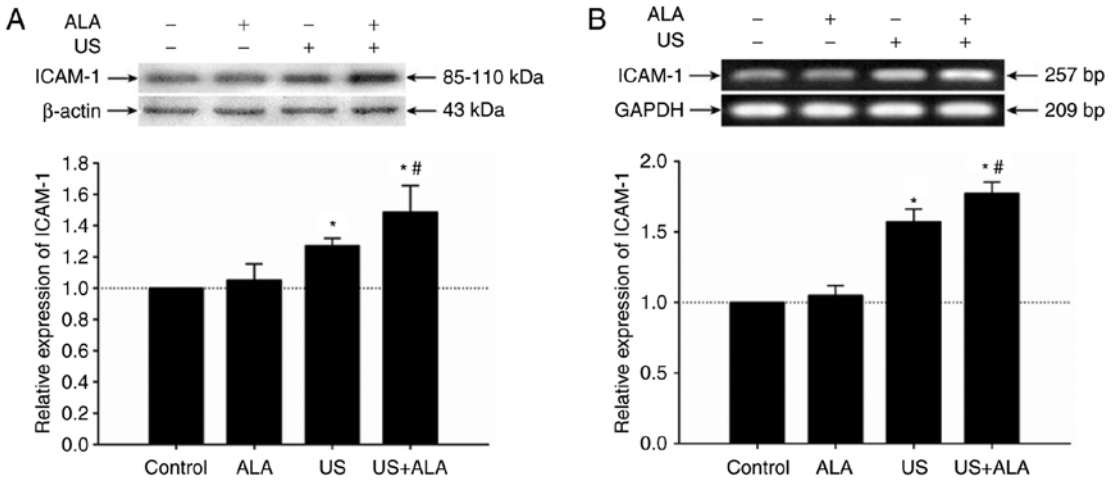

Figure 6. Effect of sonodynamic therapy on ICAM-1 expression on human umbilical vein endothelial cells. (A) Western blot analysis. (B) Reverse transcription-semi-quantitative polymerase chain reaction analysis. Data are presented as the mean ± standard deviation (n=3). *P<0.05 vs. control; #P<0.05 vs. US. US, sonication; ALA, 5-aminolevulinic acid; ICAM-1, intercellular adhesion molecule-1.

group (P=0.038; Fig. 6A). There was no significant difference between the ALA and control groups (P=0.984; Fig. 6A). In order to further confirm the results of western blotting, the mRNA level of ICAM-1 was detected by RT-sqPCR. Results demonstrated that the mRNA level of ICAM-1 was increased in US + ALA group (P<0.0001, Fig. 6B).

Discussion

SDT significantly inhibited the tumor growth and increased the survival rate in the murine xenograft model. It was demonstrated that the number of $CD45^+$, $CD68^+$ and $CD8^+$ T cells were noticeably higher in the SDT group compared with other groups. In contrast, the number of $CD4^+$ T cells did not demonstrate a significant alteration. Regulatory T cells, which are a subtype of $CD4^+$ cells, can inhibit the destruction of tumor cells by the immune system, and thus reduce immune responses. Then, the expression levels of Foxp3 and CTLA-4 proteins, which are associated with T regulatory cells were investigated.

T regulatory cell-associated Foxp3 functions as a master regulator (transcription factor) in the development and function of regulatory T cells (17,18) and is able to inhibit the activating effect of T cell receptors (19). CTLA-4 is expressed on the surface of T cells and regulates the cellular immune process. The activation of T cells to attack foreign cells occurs via the activation of CD28 receptors, and this activity is terminated by CTLA-4 (20). The results revealed that expression levels of CTLA-4 and Foxp3 decreased significantly following SDT.

During the immune process, co-stimulating molecules such as CD80 and CD86 are important adhesion molecules, expressed on antigen-presenting cells and bind with CD28 expressed on T cells (21). It is reported that the expression level of CD80, but not CD86, plays a key role in the induction of $CD4^+$ cytotoxic T cells (CTLs) (22). The results revealed that the expression levels of CD80 increased significantly following SDT. The aforementioned data demonstrated that SDT may strengthen inflammatory responses in the tumor microenvironment by limiting T regulatory cell activity, increasing the proportion of activated $CD4^+$ T cells and enhancing antigen presentation.

The enhancement and maintenance of anti-tumor immunity occurs via recognition of the tumor antigens and killing of the tumor cells, by specific CTL cells. T cells are activated in the tumor draining lymph node by corresponding tumor antigens, then are drawn to the tumor site, and adhere to the vascular endothelial cells, and migrate into the tumor microenvironment to exert antitumor immunity (23). It is well known that tumor vascular endothelial cells exhibit anergy in the tumor microenvironment, which reduces the adhesion of T cells to vascular endothelial cells, and consequently decreases the accumulation of specific T cells in the tumor microenvironment (24). The results demonstrated that compared with the control group, the number of TCVs in the SDT group decreased, and notably the lumen of TPVs was dilated with a large number of lymphocytes present. Furthermore, CD31 colocalized with ICAM-1, VCAM-1 or E-selectin respectively in the TPVs and the expression level of mRNA and protein of ICAM-1 in SDT group increased, which showed that SDT may not only activate T cells but also enhance the adhesion ability of vascular endothelial cells and thus accelerate the migration of T cells into the tumor microenvironment. The aforementioned data indicated that SDT improved the anti-tumor immune response in the murine B16F10 melanoma xenograft model. Current research regarding the impact of SDT on the immune response, particularly the adaptive immune response, is still at the initial stage (11,25,26). These results need to be verified through different tumor models in the future studies.

The present study demonstrated that SDT inhibited tumor growth, effectively activated $CD8^+$ T cells and inhibited the activity of T regulatory cells, which consequently resulted in a beneficial outcome. Furthermore, TPVs were dilated in murine xenograft and the expression of ICAM-1 was upregulated on HUVECs following SDT, which may facilitate the recruitment of immune cells. These results demonstrated that the future prospects of research on anti-tumor immunity derived from SDT are promising.

Acknowledgements

Not applicable.

Funding

The present study was supported by the National Natural Science Foundation of China (grant no. 81272503).

Availability of data and materials

The datasets used during the present study are available from the corresponding author upon reasonable request.

Authors' contributions

YP and LJ performed the xperiments, analyzed the data, wrote and edited the manuscript. SW participated in the design of methodology and completed certain experiments and data analysis. JZ and WC designed the research goals and aims, provided thoughtful discussion and edited the manuscript.

Ethics approval and consent to participate

All animal protocols were approved by the Animal Care and Use Committee of Harbin Medical University (Harbin, China).

Patient consent for publication

Not applicable.

Competing interests

The authors declare that they have no competing interests.

References

1. Rosenthal I, Sostaric JZ and Riesz P: Sonodynamic therapy - a review of the synergistic effects of drugs and ultrasound. Ultrason Sonochem 11: 349-363, 2004.
2. Shibaguchi H, Tsuru H, Kuroki M and Kuroki M: Sonodynamic cancer therapy: A non-invasive and repeatable approach using low-intensity ultrasound with a sonosensitizer. Anticancer Res 31: 2425-2429, 2011.
3. Li Y, Wang P, Zhao P, Zhu S, Wang X and Liu Q: Apoptosis induced by sonodynamic treatment by protoporphyrin IX on MDA-MB-231 cells. Ultrasonics 52: 490-496, 2012.
4. Wang X, Leung AW, Jiang Y, Yu H, Li X and Xu C: Hypocrellin B-mediated sonodynamic action induces apoptosis of hepatocellular carcinoma cells. Ultrasonics 52: 543-546, 2012.
5. Wang X, Liu Q, Wang Z, Wang P, Zhao P, Zhao X, Yang L and Li Y: Role of autophagy in sonodynamic therapy-induced cytotoxicity in S180 cells. Ultrasound Med Biol 36: 1933-1946, 2010.
6. Su X, Wang P, Yang S, Zhang K, Liu Q and Wang X: Sonodynamic therapy induces the interplay between apoptosis and autophagy in K562 cells through ROS. Int J Biochem Cell Biol 60: 82-92, 2015.
7. Lv Y, Zheng J, Zhou Q, Jia L, Wang C, Liu N, Zhao H, Ji H, Li B and Cao W: Antiproliferative and Apoptosis-inducing effect of exo-Protoporphyrin IX based sonodynamic therapy on human oral squamous cell carcinoma. Sci Rep 7: 40967, 2017.
8. Hu Z, Fan H, Lv G, Zhou Q, Yang B, Zheng J and Cao W: 5-Aminolevulinic acid-mediated sonodynamic therapy induces anti-tumor effects in malignant melanoma via p53-miR-34a-Sirt1 axis. J Dermatol Sci 79: 155-162, 2015.
9. Li Y, Zhou Q, Hu Z, Yang B, Li Q, Wang J, Zheng J and Cao W: 5-Aminolevulinic acid-based sonodynamic therapy induces the apoptosis of osteosarcoma in mice. PLoS One 10: e0132074, 2015.
10. Gao Z, Zheng J, Yang B, Wang Z, Fan H, Lv Y, Li H, Jia L and Cao W: Sonodynamic therapy inhibits angiogenesis and tumor growth in a xenograft mouse model. Cancer Lett 335: 93-99, 2013.
11. Wang S, Hu Z, Wang X, Gu C, Gao Z, Cao W and Zheng J: 5-Aminolevulinic acid-mediated sonodynamic therapy reverses macrophage and dendritic cell passivity in murine melanoma xenografts. Ultrasound Med Biol 40: 2125-2133, 2014.
12. Rosenberg SA, Spiess P and Lafreniere R: A new approach to the adoptive immunotherapy of cancer with tumor-infiltrating lymphocytes. Science 233: 1318-1321, 1986.
13. Griffith KD, Read EJ, Carrasquillo JA, Carter CS, Yang JC, Fisher B, Aebersold P, Packard BS, Yu MY and Rosenberg SA: In vivo distribution of adoptively transferred indium-111-labeled tumor infiltrating lymphocytes and peripheral blood lymphocytes in patients with metastatic melanoma. J Natl Cancer Inst 81: 1709-1717, 1989.
14. Balkwill F, Charles KA and Mantovani A: Smoldering and polarized inflammation in the initiation and promotion of malignant disease. Cancer Cell 7: 211-217, 2005.
15. Galon J, Mlecnik B, Bindea G, Angell HK, Berger A, Lagorce C, Lugli A, Zlobec I, Hartmann A, Bifulco C, *et al*: Towards the introduction of the 'Immunoscore' in the classification of malignant tumours. J Pathol 232: 199-209, 2014.
16. Lv Y, Fang M, Zheng J, Yang B, Li H, Xiuzigao Z, Song W, Chen Y and Cao W: Low-intensity ultrasound combined with 5-aminolevulinic acid administration in the treatment of human tongue squamous carcinoma. Cell Physiol Biochem 30: 321-333, 2012.
17. Tanchot C, Terme M, Pere H, Tran T, Benhamouda N, Strioga M, Banissi C, Galluzzi L, Kroemer G and Tartour E: Tumor-infiltrating regulatory T cells: Phenotype, role, mechanism of expansion in situ and clinical significance. Cancer Microenviron 6: 147-157, 2013.
18. Zhang L and Zhao Y: The regulation of Foxp3 expression in regulatory CD4(+)CD25(+)T cells: Multiple pathways on the road. J Cell Physiol 211: 590-597, 2007.
19. Marson A, Kretschmer K, Frampton GM, Jacobsen ES, Polansky JK, MacIsaac KD, Levine SS, Fraenkel E, von Boehmer H and Young RA: Foxp3 occupancy and regulation of key target genes during T-cell stimulation. Nature 445: 931-935, 2007.
20. Son CH, Bae JH, Shin DY, Lee HR, Choi YJ, Jo WS, Ho Jung M, Kang CD, Yang K and Park YS: CTLA-4 blockade enhances antitumor immunity of intratumoral injection of immature dendritic cells into irradiated tumor in a mouse colon cancer model. J Immunother 37: 1-7, 2014.
21. Sharpe AH: Mechanisms of costimulation. Immunol Rev 229: 5-11, 2009.
22. Mauri D and Pichler WJ: Involvement of CD80 in the generation of CD4+ cytotoxic T cells. Immunol Res 15: 126-140, 1996.
23. Carriere V, Colisson R, Jiguet-Jiglaire C, Bellard E, Bouche G, Al Saati T, Amalric F, Girard JP and M'Rini C: Cancer cells regulate lymphocyte recruitment and leukocyte-endothelium interactions in the tumor-draining lymph node. Cancer Res 65: 11639-11648, 2005.
24. Griffioen AW, Damen CA, Martinotti S, Blijham GH and Groenewegen G: Endothelial intercellular adhesion molecule-1 expression is suppressed in human malignancies: The role of angiogenic factors. Cancer Res 56: 1111-1117, 1996.
25. Bandyopadhyay S, Quinn TJ, Scandiuzzi L, Basu I, Partanen A, Tomé WA, Macian F and Guha C: Low-intensity focused ultrasound induces reversal of tumor-induced T cell tolerance and prevents immune escape. J Immunol 196: 1964-1976, 2016.
26. Liu HL, Hsieh HY, Lu LA, Kang CW, Wu MF and Lin CY: Low-pressure pulsed focused ultrasound with microbubbles promotes an anticancer immunological response. J Transl Med 10: 221, 2012.